Proceedings of the International School of Physics "Enrico Fermi"
Course 190 "Frontiers in Modern Optics", edited by D. Faccio, J. Dudley and M. Clerici
(IOS, Amsterdam; SIF, Bologna) 2016
DOI 10.3254/978-1-61499-647-7-77

Recent progress in weak value amplification and direct measurement

O. S. Magaña-Loaiza(*) and M. Mirhosseini

The Institute of Optics, University of Rochester - Rochester, New York, USA

R. W. Boyd

The Institute of Optics, University of Rochester - Rochester, New York, USA

Department of Physics, University of Ottawa - Ottawa, Ontario, Canada

Summary. — The ability to manipulate light has allowed scientists to verify fundamental theories of physics and to develop a new generation of technologies that use photons as a primary resource. Recent developments in quantum measurement theory have offered new alternatives to approach some of the most remarkable problems in quantum physics. Consequently, the principles of quantum mechanics have been exploited in the development of quantum technologies such as optical metrology, quantum communication, and quantum information. In recent years, weak measurements and two of its most remarkable variants: weak value amplification and direct measurement, have been developed and are considered important resources for quantum applications. In this paper, we discuss weak measurements and some significant applications of weak values. We elaborate on how distinct forms of weak values are used to observe and amplify small effects or to directly measure the quantum wave function of photons, a crucial task for schemes for quantum communication and quantum information. We also review some of the most recent methods for weak value amplification and direct measurement that our group has developed.

(*) E-mail: `omar.maganaloaiza@rochester.edu`

1. – Introduction

Bayes's theorem has played a fundamental role in classical and quantum measurement theory. As in any branch of science, the measurement process is of fundamental importance in quantum physics. However due to the nature of the formulation of quantum mechanics, different forms of measurements, or exotic implementations of statistics, have led to the observation of counterintuitive physical effects [1]. Examples include superluminal pulse propagation, the determination of the trajectory followed by a single photon in a two-slit interferometer, amplification of observables, etc. [2-8]. In addition to the fundamental character of these effects, recent work suggests that some of them could have strong implications for technological applications, such as in quantum communication, quantum information, and metrology [9-25].

In 1988 Aharonov, Albert and Vaidman introduced a generalized form of quantum measurement known as weak measurement [2]. The original paper with the title "How the result of a measurement of a component of the spin of a spin-$\frac{1}{2}$ particle can turn out to be 100" created heated debates and motivated a new generation of experiments that eventually verified the counterintuitive prediction [26,27,6,8,7,4]. In the first part of this manuscript, we discuss some of the effects that give rise to the apparent "weird" features that make weak measurements interesting and controversial, and then we describe our recent experimental contributions to this field.

2. – Weak value amplification

In this introductory part we use the von Neumann model to explain weak measurements. In this model, the total system is composed of two subsystems, one is the system we wish to measure, described by the state $|\Psi_s\rangle$, typically called the probe. The other is the pointer device $|\Psi_d\rangle$ that provides information about the measured system [1]. The correlation between these subsystems arises when the observable of the system $\hat{\sigma}$ is coupled or entangled to the pointer, through its linear momentum $\hat{p}$. This can be described by the following interaction Hamiltonian:

$$\hat{H}_{\text{int}} = g\hat{\sigma}\hat{p}, \tag{1}$$

where g is a real quantity that acts as coupling constant. The initial state can be described as the product of the state of the system or probe and the state of the pointer device as $|\Psi_i\rangle = |\Psi_s\rangle |\Psi_d\rangle$. Further, the state $|\Psi_s\rangle$ can be expressed as $\sum_n s_n |S_n\rangle$, in terms of the eigenstates of the operator $\hat{\sigma}$ as a consequence of the spectral theorem. After the interaction of duration Δt, the subsystems are coupled in the following manner:

$$|\Psi_f\rangle = e^{-i\hat{H}_{\text{int}}\Delta t} |\Psi_i\rangle = \sum_n s_n |S_n\rangle |\Psi_d(x - \chi s_n)\rangle , \tag{2}$$

where χ equals $g\Delta t$. In obtaining this result we have recalled the fact that the momentum $\hat{p}$ is the generator of translations in x. The state $|\Psi_f\rangle$ demonstrates that system and

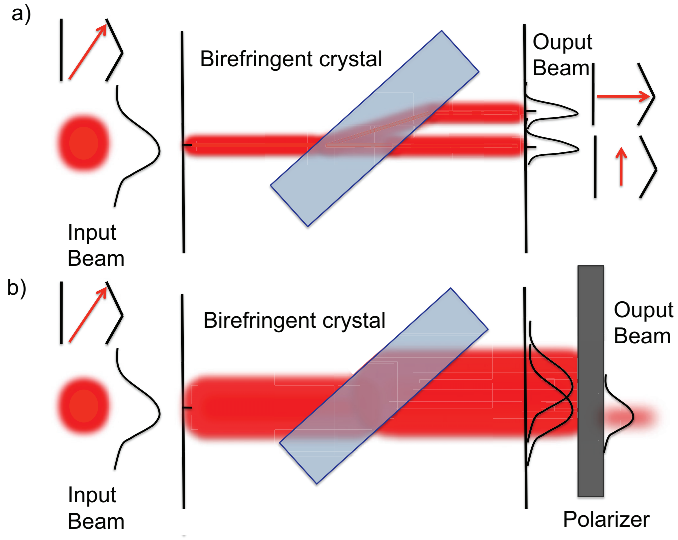

Fig. 1. – Schematic diagram of the experimental setup used to perform strong and weak measurements. a) A birefringent crystal shifts the horizontal and vertical polarized components of the input beam, which is diagonally polarized. The induced shift is larger than the beam waist diameters of the emerging beams; this strong interaction thus allows the determination of the polarization of the two beams, via strong or projective measurement. The measurement process permits one to infer information about the strength of the interaction, in this case the birefringence of the material. b) A weaker interaction between the input beam and the birefringent crystal produces a small displacement between the two emerging beams. In this case, the beam displacement is much smaller than the waist diameter of the beams. Thus it is difficult to determine the polarization of each beam. In this case, the post-selection process forces the two beams to coherently interfere, producing another beam with a Gaussian profile. When the position of the post-selection polarizer is almost orthogonal to the input polarization, the center of the post-selected beam is shifted by an amount proportional to the small separation between the two emerging beams multiplied by the weak-value amplification factor.

pointer have been coupled; this effect is sometimes referred to as entanglement [28, 29]. In addition, the position of the center of the pointer state has been shifted. If one were to calculate the expectation value of the position operator $\langle \hat{X} \rangle$ in the final state $|\Psi_f\rangle$, under ideal circumstances this will be equal to $\chi\langle\hat{\sigma}\rangle$. This result shows that the position of the pointer can be used to estimate the expectation value of the operator $\hat{\sigma}$, which explains the origin of the name of pointer. It is worth noticing that the strength of the coupling constant has not been constrained. This form of measurement is known as strong perturbative measurement [1, 2]. Typically, the probability distribution of the pointer is assumed to be a Gaussian function; however, different pointers and their advantages have been studied [30, 31]. The random noise or error associated with a measurement or read-out process is typically described by a Gaussian distribution. An example of strong measurement is depicted in fig. 1a). Here, the transverse spatial position of a Gaussian beam acts as the pointer and its polarization as the probe. The beam of light with diagonal polarization passes through a tilted birefringent crystal, which provides the interaction Hamiltonian for measuring the operator $\hat{\sigma}$. At the output of the crystal, the position and polarization of the emerging beams are well defined due to the strong interaction that occurred in the crystal, caused by its birefringence. In a typical (strong) measurement, the separation between the horizontally and vertically polarized beams is much larger than the sum of the beam waist sizes, making it easy to resolve the two beams with minimal uncertainty in the measurement of the polarization state of each photon.

In weak measurements, the initial state of the system remains mostly intact, and information is obtained by weakly disturbing the system. As a consequence, the uncertainty in each single-photon measurement is large. However, the uncertainty is generally overcome by averaging over a large number of events. The post-selection process makes weak measurements interesting. For example, the outcome of a weak measurement, called a weak value (WV), need not be an eigenvalue of the measurement operator [2, 4, 9]. In addition, WVs can be complex or exceed the eigenvalue range of a strong or projective measurement. The properties of WVs can be understood if we use the von Neumann model. In this case, we assume that the perturbation or coupling χ is small. The state after the weak perturbation can be written by expressing the interaction Hamiltonian as a power series

$$|\Psi_f\rangle = e^{-i\hat{H}_{\text{int}}\Delta t}|\Psi_i\rangle = |\Psi_s\rangle|\Psi_d\rangle - i\chi\hat{\sigma}|\Psi_s\rangle\hat{p}|\Psi_d\rangle + \dots . \tag{3}$$

After the weak perturbation, a post-selection is applied to the system. In general, the post-selection can be performed on any variable, such as polarization, linear momentum, orbital angular momentum (OAM), etc. In fact, this flexibility has allowed scientists to apply weak measurements to different scenarios and degrees of freedom [8, 12, 13, 15-21]. Therefore, our post-selection is performed by applying the projective operator $|\text{Ps}\rangle\langle\text{Ps}|$ to the state $|\Psi_f\rangle$, leading to the following state

$$|\Psi_F\rangle = |\text{Ps}\rangle\langle\text{Ps}|\,|\Psi_f\rangle = [\langle\text{Ps}|\Psi_s\rangle|\Psi_d\rangle - i\chi\langle\text{Ps}|\hat{\sigma}|\Psi_s\rangle\hat{p}|\Psi_d\rangle + \dots]\,|\text{Ps}\rangle . \tag{4}$$

Due to the weakness of the interaction, this expression can be approximated to the first order and then normalized to give

$$|\Psi_F\rangle \approx \left(|\Psi_d\rangle - i\chi\frac{\langle\text{Ps}|\hat{\sigma}|\Psi_s\rangle}{\langle\text{Ps}|\Psi_s\rangle}\hat{p}|\Psi_d\rangle\right)|\text{Ps}\rangle . \tag{5}$$

The post-selection process collapses the state of the probe, in this case $|\Psi_s\rangle$. In addition, the post-selection reveals the weak value of the operator $\hat{\sigma}$. The weak value is defined as

$$\sigma_w = \frac{\langle\text{Ps}|\hat{\sigma}|\Psi_s\rangle}{\langle\text{Ps}|\Psi_s\rangle} , \tag{6}$$

and it is important to stress that this is a general definition that can be applied to any operator defined for any degree of freedom or in any Hilbert space. Besides the collapse of the state of the system $|\Psi_s\rangle$, the post-selection process also induces a shift in the state of the pointer device $|\Psi_d\rangle$. Remarkably, this shift is proportional to the weak value and to the small disturbance χ as described by

$$|\Psi_F\rangle = |\Psi_d(x - \chi\sigma_w)\rangle\,|\mathrm{Ps}\rangle\,. \tag{7}$$

The WV σ_w can take very large values when the states $|\mathrm{Ps}\rangle$ and $|\Psi_s\rangle$ are almost orthogonal, as can be seen from eq. (6). Furthermore, when one of the coefficients of either of the two states is complex, the weak value can be complex. Such unusual features have generated a great amount of interest in weak measurements. A detailed review of this field can be found in [9].

Under many practical circumstances, weak values and weak measurements can be understood in terms of entirely classical arguments. Nonetheless, much of the recent work on weak measurements employs the simple and mathematically elegant language of quantum mechanics to describe these effects. The reason is that quantum mechanics provides a simpler description and the results apply to a wider range of phenomena than for the case of a classical description.

In 1991, Ritchie *et al.* performed the first realization of a weak value [8]. A simplified version of their experimental setup is depicted in fig. 1b). Here, we assume a weak interaction between the beam and the crystal. This interaction produces a weak coupling of the spatial profile with the polarization degree of freedom, which means that the two polarization components of the beam travel along different optical paths and become transversely separated. In this weak-interaction regime, the two beams emerging from the quartz plate are spatially separated by an amount that is much smaller than the beam waist size. For example, if one were to determine the birefringence of the material by measuring the actual position of the two beams, this will be an ineffective technique. The variance of the pointer is large, and thus the measurement will not be precise. However, the post-selection process makes this experiment interesting, since it allows discarding results that do not provide useful information and keeping those that convey relevant and conditioned information. As we will discuss, this exotic form of performing statistics can be implemented in different forms. In Ritchie's experiment the post-selection is performed with a polarizer. When the position of the post-selection polarizer is almost orthogonal to the polarization of the injected beam, the amount of transmitted light is low. Nevertheless, because of the optical interference between the two emerging beams, the spatial centroid of the post-selected beam is shifted by an amount proportional to the product of the small separation between the two beams and the weak value. So, weak values offer an alternative form of determining small quantities or weak effects.

The essence of Ritchie's experiment is shown in fig. 2. We have simulated different regimes for the experimental setup depicted in fig. 1b). We assume a beam with a Gaussian intensity distribution and a beam waist of 55 μm. The result of the constructive interference between the two beams separated by 2.5 μm is shown in fig. 2a). In fig. 2b)

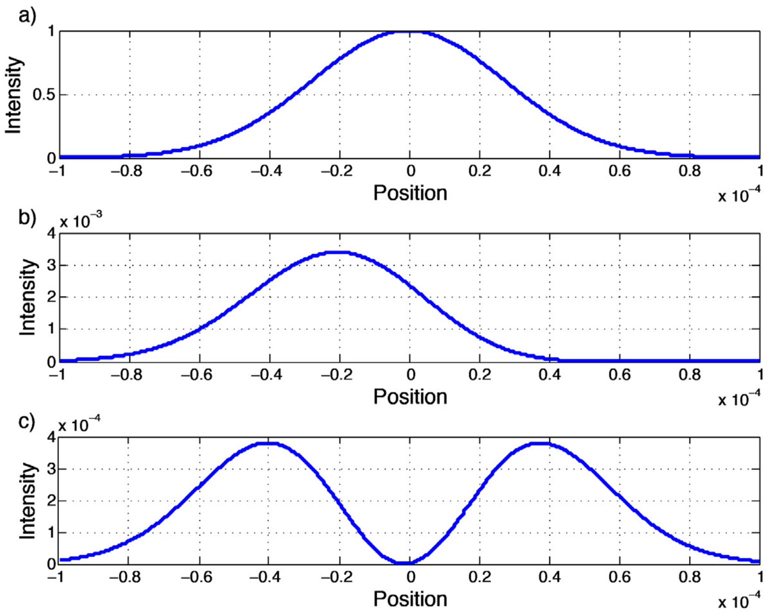

Fig. 2. – Numerical simulations that illustrate three regimes of the experimental setup depicted in fig. 1b). The transverse profile produced by constructive interference between two identical Gaussian beams with a beam waist of $55\,\mu$m separated by $2.5\,\mu$m is shown in a). One of the beams is horizontally polarized whereas the other is vertically polarized, the post-selection angle of the polarizer is 45°. b) The angle of the post-selection polarizer is set to $90° + \epsilon$ with respect to the polarization of the input beam, where ϵ equals 2.8°, this is the weak measurement regime. The shift in the pointer is proportional to the product of the weak value and the small separation between the two interfering beams. c) In this case ϵ is 0° and the weak value is not defined.

the angle of the post-selection polarizer is set to $90° + \epsilon$ with respect to the polarization of the input beam, where ϵ equals 2.8°; this is the weak measurement regime. The shift in the state of the pointer is eight times larger than the separation of the beams emerging from the crystal. This value can be increased by decreasing either ϵ or the separation between the two beams; however, the amount of light passing through the post-selection polarizer would then decrease. In fact, this is an important limitation in the protocols for weak value amplification (WVA); stronger post-selections or larger amplifications imply the loss of more photons through post selection. Furthermore, the weak value is not defined for very small values of ϵ. Figure 2c) illustrates a situation where the post-selection angle is orthogonal to the polarization of the input beam, that is, $\epsilon = 0°$.

In the work of Ritchie and co-workers, the measured weak value was real and this was measured by observing the shift in the position of the pointer. Nonetheless, as we have pointed out earlier, a weak value can be complex, and therefore one should be able to measure both the real and imaginary part of the weak value. Several authors have shown that the shift in the position and momentum of the pointer is proportional to the real and imaginary part of the weak value [32, 33], respectively.

The expectation values of the position and momentum operator for the post-selected state $|\Psi_F\rangle$ described by eq. (7) can be calculated as

$$\langle \hat{X} \rangle_F = \chi \Re \left(\frac{\langle \mathrm{Ps}| \hat{\sigma} |\Psi_s\rangle}{\langle \mathrm{Ps}|\Psi_s\rangle} \right), \tag{8}$$

$$\langle \hat{P} \rangle_F = \frac{2\chi}{\sigma^2} \Im \left(\frac{\langle \mathrm{Ps}| \hat{\sigma} |\Psi_s\rangle}{\langle \mathrm{Ps}|\Psi_s\rangle} \right). \tag{9}$$

These relations have motivated a wide variety of experiments during the last 10 years. For example, weak measurements and weak value amplification have been widely used to amplify or observe small effects in different variables. For instance, Hosten *et al.* observed the Hall effect of light, Strübi *et al.* proposed a technique to measure small time delays, Viza *et al.* measured velocities, Xu *et al.* estimated phase shifts, Dixon *et al.* measured beam deflections, Salazar-Serrano *et al.* frequency shifts and Magaña-Loaiza *et al.* angular shifts, etc. [16, 18, 13, 34, 17, 20, 19, 21]. In addition, there are several proposals that suggest that weak-value amplification can be used for metrology, although this is still a topic under discussion [14, 17, 35, 26, 27].

3. – Direct measurement

In 2011, Lundeen *et al.* proposed a technique known as direct measurement of the quantum wave function. This technique utilizes weak values to measure the wave function of a quantum particle in a direct fashion [4]. The simplicity of this technique and the fact that it does not require a time-consuming post-processing makes it attractive. The principles of quantum mechanics forbid the exact determination of the wave function of a particle in a single measurement. However, direct measurement utilizes many measurements on identically prepared systems to determine the weak values and subsequently the quantum state.

Efficient characterization of a quantum state is a crucial part of a variety of experiments in quantum optics. Recently, direct measurement has been utilized to reconstruct complicated wave functions and high-dimensional states defined on different Hilbert spaces [24, 22, 25].

The main idea behind this technique is to perform a weak measurement of the position followed it by a strong measurement of the momentum of the particle, in this case a photon. The weak value then takes the following form:

$$\pi_w = \frac{\langle p|x\rangle\langle x|\Psi_s\rangle}{\langle p|\Psi_s\rangle} = e^{ipx/\hbar} \frac{\Psi_s(x)}{\Phi(p)}. \tag{10}$$

As can be seen, the weak value takes a different form to the one obtained in protocols for weak value amplification. Furthermore, if the post-selection is carried out at $p = 0$,

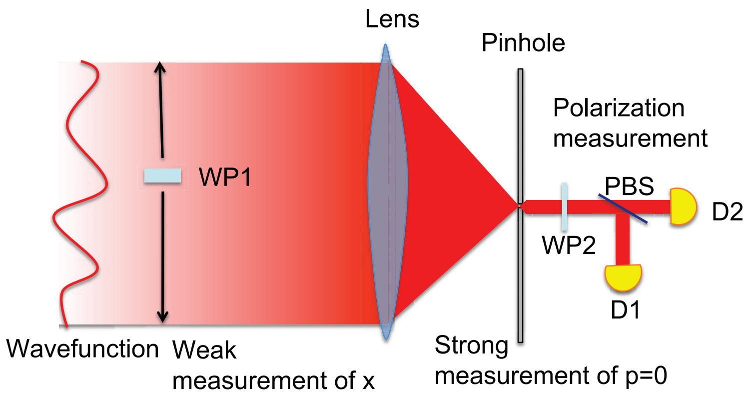

Fig. 3. – Experimental apparatus used by Lundeen and co-workers to measure the spatial wave function of a single photon [4]. A weak rotation of polarization, via HWP (WP1) is followed by a strong measurement of the momentum. A series of polarization measurements allow the reconstruction of the spatial quantum wave function.

the expression above can be simplified to

$$\pi_w = k\Psi_s(x), \tag{11}$$

where k is equal to $1/\Phi(0)$ which can be considered to be a normalization constant. This remarkable result shows that this recipe produces a weak value that is directly related to the transverse quantum wave function of the measured photons.

The experimental implementation of this method used the relatively simple apparatus depicted in fig. 3. The complete technique comprises three stages. The first part can be understood as a weak measurement in the position variable. This measurement is performed by using a rectangular sliver of a half-wave plate (HWP), labeled it as WP1, to weakly rotate the polarization of light at a specific position. A Fourier transforming lens and a small pinhole allows one to perform the post-selection at $p = 0$ in the momentum basis. The last part is the strong measurement process. Here a HWP or a quarter wave plate (QWP), labeled as WP2, together with a polarizing beam splitter (PBS) permits the measurement of the real or imaginary part of the WV, respectively.

The interaction Hamiltonian that describes the effect of the weak disturbance in the position variable is $H_{\text{int}} = \alpha\hat{\sigma}_y\hat{\pi}$, where α is a small polarization rotation angle, $\hat{\sigma}_y$ is one of the Pauli matrices defined as $-i\left|H\right\rangle\left\langle V\right| + i\left|V\right\rangle\left\langle H\right|$ and $\hat{\pi}$ is the position operator $\left|x\right\rangle\left\langle x\right|$. After the post-selection at $p = 0$, the final state (which can be described as in eq. (5)) takes the following form

$$\left|s_f\right\rangle = \left|V\right\rangle + \frac{i\alpha}{2}\pi_w\hat{\sigma}_y\left|V\right\rangle. \tag{12}$$

It is important to point out that the above state provides information about the wave function only at a specific position x. In order to retrieve the full wave function, one has to repeat this measurement at various positions x. After the operator $\hat{\sigma}_y$ is applied to the polarization state, $|s_f\rangle$ takes the form

$$|s_f\rangle = |V\rangle + \frac{\alpha}{2}\pi_w |H\rangle . \tag{13}$$

Since the pointer is the polarization degree of freedom, in order to reconstruct the quantum wave function one has to fully characterize the polarization of the detected photons. One way of doing this is by measuring the Pauli operators $\hat{\sigma}_x$ and $\hat{\sigma}_y$ in the final state $|s_f\rangle$. Notably, measurement of $\langle s_f| \hat{\sigma}_x |s_f\rangle$ provides information about the real part of the weak value

$$\begin{aligned} \langle s_f| \hat{\sigma}_x |s_f\rangle &= \langle s_f| (|H\rangle \langle V| + |V\rangle \langle H|) |s_f\rangle \\ &= \alpha\Re[\pi_w]. \end{aligned} \tag{14}$$

The state above can be measured by using a HWP for WP2 and a PBS. In addition, replacing the HWP with a QWP allows the measurement of the Pauli operator $\hat{\sigma}_y$, which is proportional to the imaginary part of the weak value

$$\begin{aligned} \langle s_f| \hat{\sigma}_y |s_f\rangle &= \langle s_f| (-i |H\rangle \langle V| + i |V\rangle \langle H|) |s_f\rangle \\ &= -\alpha\Im[\pi_w]. \end{aligned} \tag{15}$$

Therefore the wave function can be reconstructed from the measurements of $\langle s_f| \hat{\sigma}_x |s_f\rangle$ and $\langle s_f| \hat{\sigma}_y |s_f\rangle$ as follows:

$$\Psi_s(x) = \frac{1}{k\alpha}(\langle s_f| \hat{\sigma}_x |s_f\rangle - i \langle s_f| \hat{\sigma}_y |s_f\rangle). \tag{16}$$

In the following section, we describe some experimental implementations that utilize weak values for amplification of small effects and direct measurement of wave functions in various Hilbert spaces.

4. – Experimental weak measurements

Our discussion starts with weak-value amplification in the azimuthal degree of freedom [21]. We then describe three implementations of direct measurement; compressive direct measurement of the quantum wave function [25], direct measurement of a 27-dimensional orbital angular momentum state [22] and the full characterization of polarization states of light via direct measurement [24].

Weak value amplification in angular position and OAM variables. – Besides the extensive work on the estimation of longitudinal displacements [36, 19, 14, 37, 38, 17], high-sensitivity measurement of angular displacements has been a recent topic of interest. Notably, light carrying orbital angular momentum has became the most popular resource for this purpose. As identified by Allen *et al.* [39], an optical beam with azimuthal phase dependence of the form $e^{i\ell\phi}$ carry OAM; here, ϕ is the azimuthal angle and ℓ is the OAM value. These beams have been used for rotational control of microscopic systems and exploration of effects such as the rotational Doppler shift [40], which has been recently used for detecting spinning objects [41]. Recent efforts to increase the sensitivity in the measurement of angular rotations involve the generation of large values of OAM [42], quantum entanglement of high OAM values [43], and the use of N00N states in OAM bases [44]. These protocols require complicated schemes to generate and measure photons in such exotic states. However, the ultimate realization of such methods could result in significant improvements in optical metrology, remote sensing, biological imaging, and navigation systems.

We describe WVA in the azimuthal degree of freedom and the processes that give rise to these effects. The first observation of these WVs is interesting from the point of view of fundamental physics and potential applications. For instance, the spin-orbit coupling gives rise to an optical effect in which the perturbation of polarization induces a shift in the angular position and OAM spectrum of the pointer. We demonstrate that the real and the imaginary part of the WV for a polarization operator can be accessed by measuring the angular position and its conjugate variable, of OAM. Using a new variation of WVs based on spin-orbit coupling, we propose a scheme for the measurement of small rotations. An amplification in the measurement of angular rotations that is as large as 100 is demonstrated [21]. The simplicity of the scheme, and the lack of need for exotic quantum states or extremely large OAM values, make this technique attractive for applications in optical metrology and remote sensing.

The experimental setup is depicted in fig. 4. The polarization and spatial profile of the beam are used as probe and pointer, respectively. The initial polarization state is selected using a polarizer and a HWP, that are labeled as WP1; this state can be described by the polarization qubit $|\Psi_{\mathrm{pr}}\rangle = \frac{1}{\sqrt{2}}(|H\rangle + |V\rangle)$. The preparation of the spatial mode [45] consists of the generation of an angular mode (ANG) $f(\phi) \propto \exp\left(-\phi^2/2{\eta_\phi}^2\right)$, which is a Gaussian angular slit of width η_ϕ. The beam is injected into a Sagnac interferometer, where the horizontally and vertically polarized components of the beam circulate in opposite directions. The dove prism (DP) is rotated by a small angle $\Delta\phi/4$ with respect to the plane of the interferometer, which causes the two counter-propagating beams to be rotated by an amount of $\pm\Delta\phi/2$ in opposite directions. The interferometer couples the polarization, marked by the two counter-propagating beams, and the transverse azimuthal degree of freedom. Two QWPs and a HWP, labeled as WP2, are used to induce a geometric phase between the two circulating beams in the interferometer, permitting the existence of complex WVs. The angle of the QWPs is set to $\pi/4$ and the angle of the HWP defines the geometric phase. Finally, the post-selection is performed

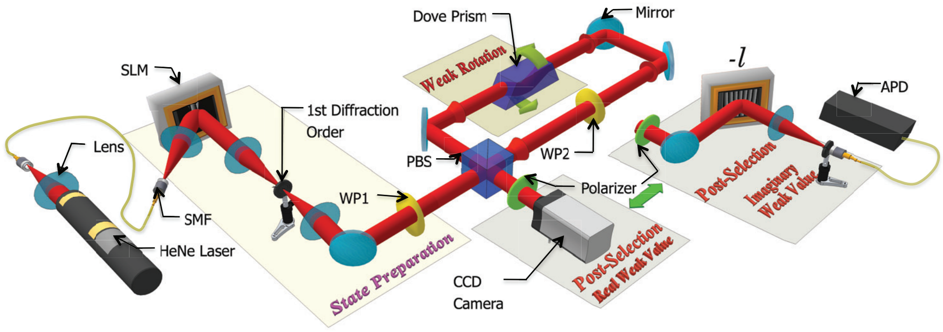

Fig. 4. – Experimental setup. A HeNe laser working at 632.8 nm is coupled into a single-mode fiber (SMF) and the output is then collimated. The beam is sent to a spatial light modulator (SLM) and then to a $4f$ optical system containing a spatial filter in the Fourier plane. This permits one to shape the angular Gaussian slit onto the beam. A polarization qubit is prepared by means of a polarizer and a HWP, that are labeled as WP1. A dove prism (DP), a HWP and two QWPs are placed inside the Sagnac interferometer; the waveplates are labeled as WP2. The DP induces a small rotation between the counter-propagating beams; this is the weak perturbation. The waveplates in WP2 induce a geometric phase between the H and V polarized beams. After post-selection, measurements of angular positions and OAM spectra are performed to access the real and imaginary parts of the weak value.

by setting the angle of a polarizer almost orthogonal with respect to the angle of the polarizer used for pre-selection. At this stage, the measurement of the complex wave function in the transverse angular basis and in the conjugate basis of OAM provides information regarding the real and the imaginary part of the WV, respectively.

The state at the input of the interferometer has the form $|\Psi_i\rangle = |\Psi_{\rm pr}\rangle\,|f(\phi)\rangle$, which is the product of the polarization state of the probe and the spatial profile of the pointer. The state at the output of the interferometer is

$$|\Psi_f\rangle = \frac{1}{\sqrt{2}}\left(e^{-i\frac{\theta}{2}}\,|H\rangle\,|f(\phi-\Delta\phi/2)\rangle + e^{i\frac{\theta}{2}}\,|V\rangle\,|f(\phi+\Delta\phi/2)\rangle\right), \tag{17}$$

where θ is defined as $\theta_H-\pi$, and θ_H is the induced geometric phase, which is set by the angle of the HWP in WP2. The post-selection is performed by projecting the perturbed state onto $|\Phi_{\rm ps}\rangle = \sin\left(\frac{\gamma}{2}-\frac{\pi}{4}\right)|H\rangle + \cos\left(\frac{\gamma}{2}-\frac{\pi}{4}\right)|V\rangle$, where γ is controlled by the angle of the post-selection polarizer. The post-selection collapses the polarization state of the probe and causes a shift in the angular position and the OAM spectrum of the pointer; this can be described as

$$|\Psi_p\rangle = |\Phi_{\rm ps}\rangle\,\langle\Phi_{\rm ps}|\,\Psi_f\rangle \approx |\Phi_{\rm ps}\rangle\,|f(\phi-\sigma_w\Delta\phi/2)\rangle\,. \tag{18}$$

Here, σ_w is the complex WV, given by

$$\sigma_w \equiv \frac{\langle\Phi_{\rm ps}|\,\hat\sigma\,|\Psi_{\rm fpr}\rangle}{\langle\Phi_{\rm ps}|\,\Psi_{\rm fpr}\rangle}\,. \tag{19}$$

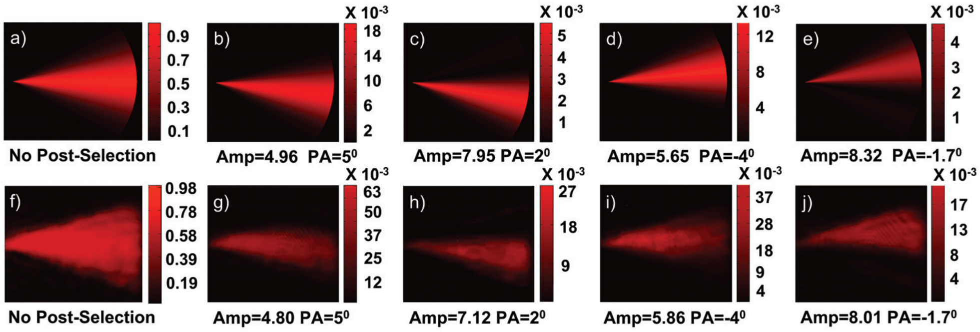

Fig. 5. – Real weak value amplification of angular rotations. Panels a)-e) show simulations of the experiment for $\Delta\phi = 1.2°$ and different post-selection angles (PA) and amplification factors (Amp). Panels f)-j) show experimental evidence of our protocol under similar conditions (figure adapted from ref. [21]).

The action of the polarization-sensitive Sagnac interferometer is described by $\hat{\sigma}$, which is defined as $|H\rangle\langle H| - |V\rangle\langle V|$, and $|\Psi_{\mathrm{fpr}}\rangle$ is described as $\frac{1}{\sqrt{2}}\left(e^{-i\frac{\theta}{2}}|H\rangle + e^{i\frac{\theta}{2}}|V\rangle\right)$. $|\Psi_{\mathrm{fpr}}\rangle$ represents the final state of the probe, after the induced geometric phase. If θ and $\gamma/2$ are small, the WV can be approximated as

$$\sigma_w \approx -\frac{2\gamma}{\gamma^2+\theta^2} + i\frac{2\theta}{\gamma^2+\theta^2}\,. \tag{20}$$

The post-selected state described in eq. (18) shows a change in angle as $\phi \to \phi - \sigma_w\Delta\phi/2$; then

$$f(\phi - \sigma_w\Delta\phi/2) = e^{\left(-(\phi-\sigma_w\Delta\phi/2)^2/2\eta_\phi^2\right)} \propto e^{\left(-(\phi-\Delta\langle\phi\rangle)^2/2\eta_\phi^2\right)}e^{(i\phi\Delta\langle\ell\rangle)}, \tag{21}$$

where $\Delta\langle\phi\rangle = \Re(\sigma_w)\Delta\phi/2$ sets the amount of the pointer's rotation. In addition, the pointer experiences a shift in its OAM spectrum that equals $\Delta\langle\ell\rangle = \Im(\sigma_w)\Delta\phi/2\eta_\phi^2$. The shift in the OAM spectrum can be understood as an interaction between spin angular momentum (SAM) and OAM. This optical effect is a consequence of the polarization-sensitive nature of the interactions occurred in the interferometer, and it is not related to the standard spin-orbit coupling in the vector beams where both of the spin and the orbital angular momenta are directed along the same axis [46].

In this experiment, a 3 mW HeNe laser (632.8 nm) is coupled to a single-mode fiber (SMF) and then expanded. The DP inside the Sagnac interferometer is rotated by 0.3°. The induced displacement $\Delta\phi$ is chosen to be much smaller than the width of the ANG mode. The post-selection polarizer is set to an angle $\gamma/2$ with respect to the polarization state of the pre-selected state. For the first part, θ is set to zero. The post-selection polarizer forces the two ANG modes to coherently interfere, producing a rotated ANG mode [8]. The rotation is proportional to the angular displacement $\Delta\phi$ and the real part

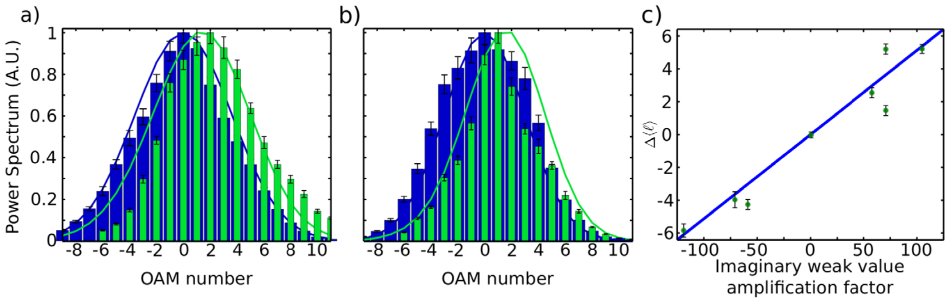

Fig. 6. – OAM power spectra of the pointer without post-selection (blue) and with post-selection (green) demonstrating the shift in $\langle \ell \rangle$ due to $\Im(\sigma_w)$ for a) $\eta_\phi = 11.4°$, $\gamma/2 = 6°$ and b) $\eta_\phi = 13.7°$ and $\gamma/2 = 5°$. The angle $\theta/2$ equals $5°$ for all the cases. The histograms represent measured data, whereas lines represent theoretically predicted shifts. c) OAM centroid shift $\Delta\langle \ell \rangle$ for various measured OAM power spectra plotted against the imaginary WV amplification factor, $\Im(\sigma_w)/2{\eta_\phi}^2$. Dots represent data, and the line is the theoretical linear curve predicted by eq. (7), (figure adapted from ref. [21]).

of the WV $\Re(\sigma_w)$. Since the WV takes values larger than one, this protocol allows the amplification of small rotations. However, as $\Re(\sigma_w)$ is increased more photons are lost; this is shown for different post-selection angles (PA) in fig. 5.

As shown in eq. (21), one can access to the imaginary part of the WV by analyzing the shift of the OAM spectrum of the pointer. In order to have complex WVs, the phase θ has to be nonzero. The HWP in WP2 is therefore set to an angle such that $\theta/2 = 5°$ and we used different post-selection angles for the polarizer. For simplicity, the OAM spectrum is measured by using projective measurements for various values of ℓ.

As predicted by eq. (21), and shown in fig. 6, larger amplifications are obtained for angular modes with narrow widths. However, such narrow ANG modes have physically smaller cross sections, and hence they proportionally carry less power. As shown in fig. 6c), by exploiting the measurement process, small rotations are amplified by a magnitude of 100 without using high OAM or nonclassical states of light.

This scheme represents the first step towards the study and understanding of WVA in the azimuthal degree of freedom. We describe the physical mechanisms that produce a shift in the angular position and OAM of an optical beam. The shift in the OAM spectrum is a consequence of the breakup in the polarization symmetry, realized by a differential geometric phase. These results provide a proof-of-principle demonstration of the scope of WVA in this degree of freedom.

Compressive direct measurement of the transverse wave function. – We now describe recent experiments related to the direct measurement of the wave function. We start this section by introducing a technique called compressive direct measurement (CDM) [25]. This scheme combines the benefits of direct measurement with a computational technique known as compressive sensing (CS) [47, 48]. CS uses a nonlinear algorithm to recover a sparse n-dimensional signal from a series of m projective measurements. Unlike the case of linear reconstruction, the number of measurements m in a compressive scheme can be much smaller than the dimension n of the signal. CS provides an efficient alternative to raster scanning in the application where arrayed-detectors are either costly or not available such as quantum optics and low-light-level measurements. Specific examples include single-photon level imaging, entanglement characterization, and quantum ghost imaging [49-55].

We use the polarization of the photon as the pointer. The initial system-pointer state can be written as

$$|\Omega\rangle = |\psi\rangle\,|V\rangle = \sum_{i=1}^{N} \psi_i\,|x_i\rangle\,|V\rangle\,, \tag{22}$$

where $|V\rangle$ indicates that the initial polarization is vertical and where $|\psi\rangle$ is the initial spatial wave function. We next perform a series of random weak measurements in order to retrieve the spatial wave function $|\psi\rangle$. Each measurement is described by the projection operator $\hat{Q}_m$, that can be expanded as a weighted sum of position projection operators $\hat{\pi}_j$ at all the points

$$\hat{Q}_m = \sum_j Q_{m,j}\hat{\pi}_j. \tag{23}$$

For the purpose of simplifying the experiment we consider the special case where $Q_{m,j}$ a real coefficient that can be either 1 or 0. The state of the particle after the measurement can be approximately described as

$$e^{i\alpha}\,|\Omega\rangle \approx |\Omega\rangle + \alpha\sum_{i=1}^{N} Q_{m,j}\psi_i\,|x_i\rangle\,|H\rangle\,. \tag{24}$$

Following the weak measurement, we perform a projection onto the zeroth order momentum state. This will erase the spatial structure of the photons and we are left with a beam with the polarization state

$$|s_m\rangle = |V\rangle + \frac{\alpha}{\phi_0\,\sqrt{N}}\sum_j Q_{m,j}\psi_j\,|H\rangle\,. \tag{25}$$

At this stage the information about the state-vector ψ_j is encoded in the expected values of the polarization of the post-selected state

$$\begin{aligned} \bar{\sigma}_{x,m} &= \langle s_m|\,\hat{\sigma}_x\,|s_m\rangle = k\sum_j Q_{m,j}\Re[\phi_j], \\ \bar{\sigma}_{y,m} &= \langle s_m|\,\hat{\sigma}_y\,|s_m\rangle = -k\sum_j Q_{m,j}\Im[\phi_j], \end{aligned} \tag{26}$$

where $\hat{\sigma}_x = |H\rangle\langle V| + |V\rangle\langle H|$, $\hat{\sigma}_y = -i|H\rangle\langle V| + i|V\rangle\langle H|$ and $\kappa = \frac{2\alpha}{\phi_0\sqrt{N}}$. After repeating the measurement M times, one obtains a linear relation between the measurement results and the unknown wave function

$$\begin{pmatrix} \phi_1 \\ \phi_2 \\ \vdots \\ \phi_M \end{pmatrix} = \begin{pmatrix} Q_{1,1} & Q_{1,2} & \cdots & Q_{1,N} \\ Q_{2,1} & Q_{2,2} & \cdots & Q_{2,N} \\ \vdots & \vdots & \ddots & \vdots \\ Q_{M,1} & Q_{M,2} & \cdots & Q_{M,N} \end{pmatrix} \begin{pmatrix} \psi_1 \\ \psi_2 \\ \vdots \\ \psi_N \end{pmatrix}. \tag{27}$$

Here, $\phi_m = \frac{1}{\kappa}[\bar{\sigma}_{x,m} - i\bar{\sigma}_{y,m}]$, and $m \in \{1 : M\}$ and $n \in \{1 : N\}$, where M is the number of times the measurement is repeated with different random projections. For the case where $M = N$, the solutions of the system above can be exactly solved for a non-singular matrix $\hat{Q}$. However, for the case when $M \leq N$ there exists multiple (and typically many, for small Ms) solutions to the system of equation.

Compressive sensing provides a method for finding the solution by using the prior knowledge of sparsity of the unknown function in a known basis. This is often achieved by solving an optimization problem that can be formulated in multiple forms. In our experiment, we assume sparsity in the gradient basis, which leads to the following optimization problem

$$\min_{\psi'} \sum_j ||\nabla\psi'_j||_{l_1} + \frac{\mu}{2}||\hat{Q}\psi' - \phi||^2_{l_2}. \tag{28}$$

Here, $\nabla\psi'$ is the discrete gradient of ψ' at position x_j, and μ is a weighting factor that penalizes deviations from experimental data. Heuristically, the solution of the optimization problem allows the determination of the *smoothest* state ψ', that is *approximately* in agreement with the experimental data.

Figure 7 shows the schematic of the experiment. A vertically polarized Gaussian beam illuminates a SLM, which together with two QWPs (WP1 and WP2) performs the polarization rotation. The amount of rotation can be controlled at each pixel by setting the grayscale values on the SLM. After the Fourier transforming lens, the post-selection in the momentum basis is performed by using a pinhole that projects on a single spatial mode. As derived in sect. **3**, the real part of the WV is retrieved by using a HWP (shown as WP3 in fig. 7) and a PBS. Similarly, the imaginary part of the WV is measured by using a QWP before the PBS. The flux of photons at the two output ports of the PBS are detected with APDs.

For each measurement m, a pre-generated random binary matrix $\hat{Q}_m$ is displayed on the SLM. The photon fluxes measured at the APDs are used to find the expectation values of the Pauli matrices for each measurement and subsequently ϕ_m. The wave function is then retrieved via post processing on a computer. We use the algorithm known as Total Variation Minimization by Augmented Lagrangian and Alternating Direction [56] (TVAL3) to solve eq. (25).

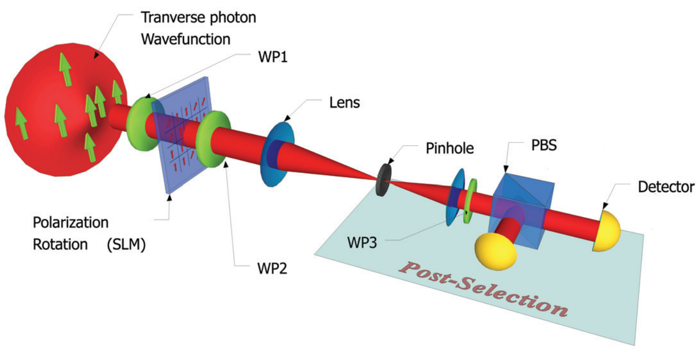

Fig. 7. – A collimated vertically polarized Gaussian beam illuminates a SLM, which is used along with two QWPs (WP1and WP2) to rotate the polarization at each pixel. A lens focuses the beam onto a pinhole with a diameter of $10\,\mu$m. The polarization measurement is performed on the light collected from the pinhole using a QWP/HWP (WP3) and a PBS.

We perform the experiment on an aberrated Gaussian beam. This corresponds to a complex wave function with non-trivial real and imaginary parts. First, the wave function is reconstructed via standard direct measurement. The real and imaginary parts from a pixel-by-pixel raster scan are shown on the left column of fig. 8 for an $N = 12 \times 16 = 192$ dimensional Hilbert space. On the middle column, we have shown the real and imaginary parts of the wave function reconstructed from CDM using $N = 192$

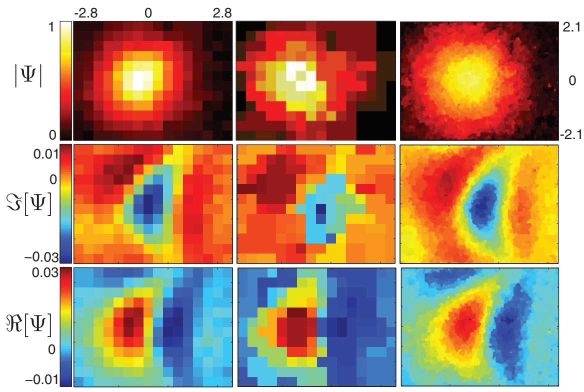

Fig. 8. – The amplitude, real, and imaginary parts of an aberrated Gaussian state measured experimentally. The left column shows data from a pixel-by-pixel scan of the state for $N = 192$. The middle column presents the reconstructed wavefront for $N = 192$, and $M/N = 20\%$ of total measurements from the CDM method. The right column demonstrates reconstruction of a higher dimensional state for $N = 19200$, and $M/N = 20\%$ of total measurements. The transverse dimensions of the state are shown in millimeters (figure adapted from ref. [25]).

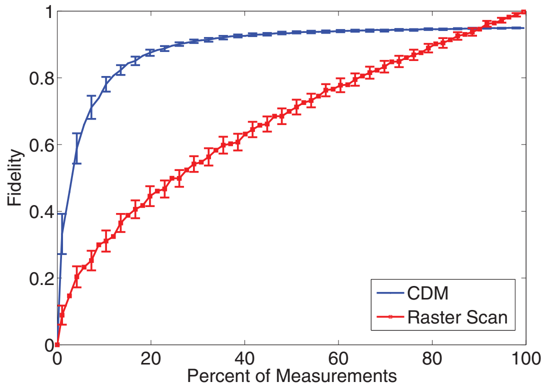

Fig. 9. – The fidelity of the reconstructed state with the target wave function as a function of the percentage of total measurements for a 192 dimensional state. The fidelity of the state reconstructed with CDM is shown in blue. The fidelity of the retrieved state from a partial pixel-by-pixel scan with the same number of measurements is shown in red. The error-bars represent standard deviation calculated from 100 repetitions of the experiment (figure adapted from ref. [25]).

and $M/N \times 100 = 20\%$. It is evident that a reconstruction with 20% of measurements can find all the main features of the wave function. Nevertheless, a high quality reconstruction requires a more sparse signal. To achieve this, we use a smaller pixal size. This results in a wave function with a larger dimension size. Moreover, the increased sampling results in a more sparse representation in the gradient basis. On the right column of fig. 8 the reconstructions for $N = 120 \times 160 = 19200$ and $M/N \times 100 = 20\%$ are shown. It can be seen that an experiment with 20% of measurements provides an accurate reconstruction.

We use fidelity as a metric for quantifying our results. For a pair of pure states, fidelity is defined as

$$F(|\psi'\rangle, |\psi\rangle) = |\langle\psi'|\psi\rangle|. \tag{29}$$

Here, the retrieved state $|\psi'\rangle$, via CDM, is compared with the target state $|\psi\rangle$ that is retrieved from standard direct measurement. The results are shown in fig. 9. The horizontal axis represents the percentage of measurements. The blue line shows the fidelity of the retrieved state with the CDM method. The red curve represents the average fidelity of the reconstructed state using the data from a partial pixel-by-pixel measurement. It is remarkable that the compressive method results in a drastic increase of fidelity for the first few measurements and gradually settles to a value close to 1. For example, a fidelity as high as 90% is achieved by performing 25% of measurements, while the standard direct measurement (this is, a raster scan) requires of approximately 80% of all the measurements to achieve the same fidelity.

The measurement of the quantum wave function has been one of the great experimental challenges in quantum physics. Over the past 20 years, many seminal contributions have been made to this field [57, 58]. Despite this achievements, the reconstruction of high-dimensional states remains challenging. The direct measurement approach, introduced by Lundeen *et al.*, has provided a straight-froward experimental techniques that can be easily adopted for measuring multi-level states. We have introduced the compressive direct measurement as an efficient and fast technique for the direct measurement of quantum wave functions with very large dimensions. In addition to quantum optics, our technique can be used for application in classical regimes were an array of detectors is not available, such as the imaging and wavefront sensing with Terahertz waves.

Direct measurement of a 27-dimensional OAM state. – Another remarkable application of direct measurement is the characterization of a high-dimensional state in the discrete basis of OAM [22]. The measurement of the OAM of light is considered an important tool in the machinery of quantum optics [59-62], especially due to the wide variety of applications that light endowed with OAM has found [63-66, 41, 46, 59, 42]. We determine the probability amplitudes of a pure state by performing a weak measurement of OAM and strong measurement of angular position. Remarkably, all the difficulties of determining information of a state in the OAM basis can be reduced to performing simple polarization measurements.

In a form similar to that by which a qubit is defined in the polarization degree of freedom, a qudit can be defined in the OAM basis. For example, one can prepare a photon in the following superposition:

$$|\Psi\rangle = \sum_{\ell} a_{\ell} |\ell\rangle \,, \tag{30}$$

where the coefficients a_{ℓ} are complex probability amplitudes and $|\ell\rangle$ is an eigenstate of OAM with eigenvalue ℓ. Similar to linear position and linear momentum, the angular position and OAM of a photon form a discrete Fourier conjugate pair [67]. Therefore, an ANG mode $|\theta_n\rangle$ can be defined as an equally weighted superposition of OAM states as $\frac{1}{\sqrt{2\ell_0+1}}\sum_{\ell=-\ell_0}^{\ell_0}\exp(\frac{i2\pi n\ell}{2\ell_0+1})\,|\ell\rangle$; thus the OAM states $|\ell\rangle$ are mutually unbiased with respect to the states in the angular position basis $|\theta\rangle$; consequently, the inner product of each pair of OAM and ANG has the same magnitude. Thus, one can define the quantity $c = \langle\theta_0|\ell\rangle/\langle\theta_0|\Psi\rangle$, which is a constant with respect to $|\ell\rangle$ when $\theta_0 = 0$. If $|\Psi\rangle$ is multiplied by this constant, one can expand it as

$$c\,|\Psi\rangle = c\sum_{\ell}|\ell\rangle\,\langle\ell|\Psi\rangle = \sum_{\ell}|\ell\rangle\,\frac{\langle\theta_0|\ell\rangle\langle\ell|\Psi\rangle}{\langle\theta_0|\Psi\rangle} = \sum_{\ell}\langle\pi_{\ell}\rangle_w\,|\ell\rangle\,, \tag{31}$$

where $\hat{\pi}_{\ell}$ is the OAM projection operator $|\ell\rangle\,\langle\ell|$ and $\langle\pi_{\ell}\rangle_{\mathrm{w}}$ is the OAM weak value. Therefore, by performing a weak measurement of the OAM followed by a strong measurement in the angular position, one can obtain enough information to reconstruct the wave function in the angular basis. After post-selection, the final state has the final form shown in eq. (13), so the weak value $\langle\pi_{\ell}\rangle_{\mathrm{w}}$ can be determined as in eq. (22) by implementing the same polarization measurements.

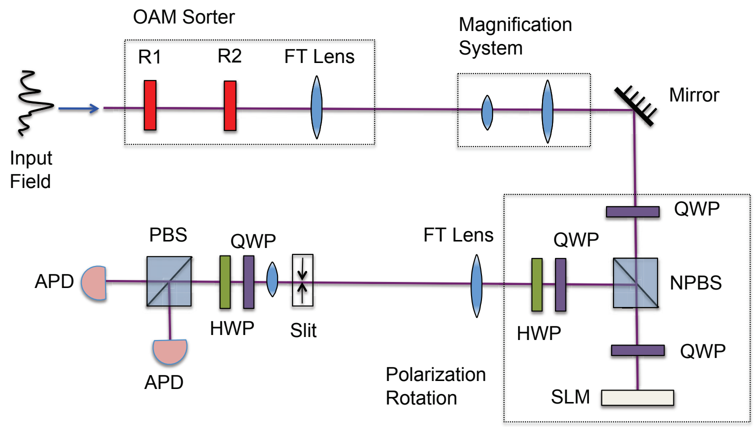

Fig. 10. – Simplified schematic of the experimental setup to directly measure the wave function of a photon in the OAM basis. The mode sorter converts an OAM mode to a plane wave with a tilt that is proportional to the OAM quantum number ℓ. The unwrapped mode is Fourier transformed by a lens to position modes that are magnified. The actual perturbation occurs when the polarization of the mode is rotated by a small amount; this step is performed by an SLM and two QWPs. The post-selection or strong measurement of angular position is performed by a rectangular slit, placed after a Fourier-transforming lens. As in the previous protocols, a series of polarization measurements, that involves the use of a HWP or QWP, allows for the reconstruction of the complex wave function.

The experimental procedure for this protocol is depicted in fig. 10. The spatial profile of the input field is prepared by encoding a wedge-shaped mask onto an SLM; this procedure generates a sinc distribution of OAM probability amplitudes. The polarization of the shaped beam is vertical. The mode sorter converts an OAM mode to a plane wave with a tilt that is proportional to the OAM quantum number ℓ. The unwrapped mode is Fourier transformed by a lens to position modes. This is the first step in performing the weak perturbation of the OAM projection operator. The actual perturbation occurs when the polarization of the mode is rotated by a small amount; this step is performed by an SLM and two QWPs. The post-selection or strong measurement of angular position is performed by a rectangular slit, placed after a Fourier-transforming lens. As in the previous protocols, a series of polarization measurements allows for the reconstruction of the complex wave function.

Figure 11 shows the experimental results of this experiment. The real and imaginary parts of the wave function from the experiment are shown in fig. 11a). The probability density $|\Psi(\ell)|^2$ and the phase $\phi(\ell)$ are calculated in fig. 11b) and c), respectively. In addition, the ability to measure the phase of the state allows one to measure rotations in the OAM basis. Malik *et al.* demonstrate that this method permits one to directly observe the phase acquired by the state after an angular rotation; in standard protocols that do not use weak value this determination must be performed indirectly through interferometric techniques. The acquired phase $i\ell\theta$ increases with the OAM quantum number ℓ.

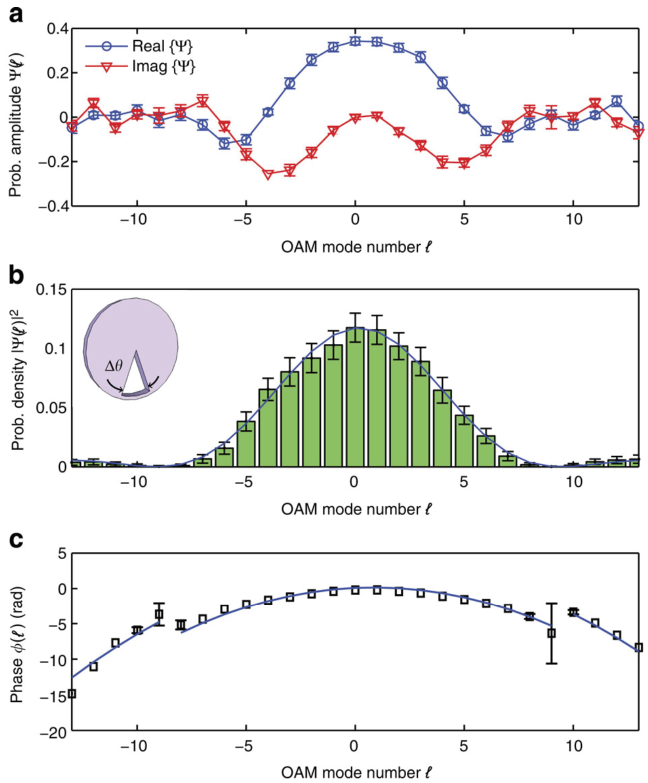

Fig. 11. – Experimental data showing complete information of a 27-dimensional quantum state in the OAM basis. The prepared state is given by the OAM spectrum of the angular aperture shown in the inset of (b). (a) The measured real and imaginary parts of the quantum wave function. (b) The measured probability distribution of the prepared state. (c) The measured phase of the state (figure adapted from ref. [22]).

This experiment demonstrates the full characterization of a quantum state in the OAM basis, a task that started more than 10 years ago with the measurement of orbital angular momentum of a single photon [60]. It is important to stress the potential and flexibility of direct measurement. In general, it can be applied to any degree of freedom. However, the difficulty of the experiment depends on the involved variables or degrees of freedom. For instance, in order to measure the quantum wave function in the OAM basis, a log-polar to linear coordinate transformation, performed by the OAM sorter, was required [61].

Full characterization of polarization states of light via direct measurement. – The last experiment we will describe here is the full characterization of polarization states of light via direct measurement. Here, Salvail *et al.* reconstruct the wave function of a qubit system and its density matrix via direct measurement [24].

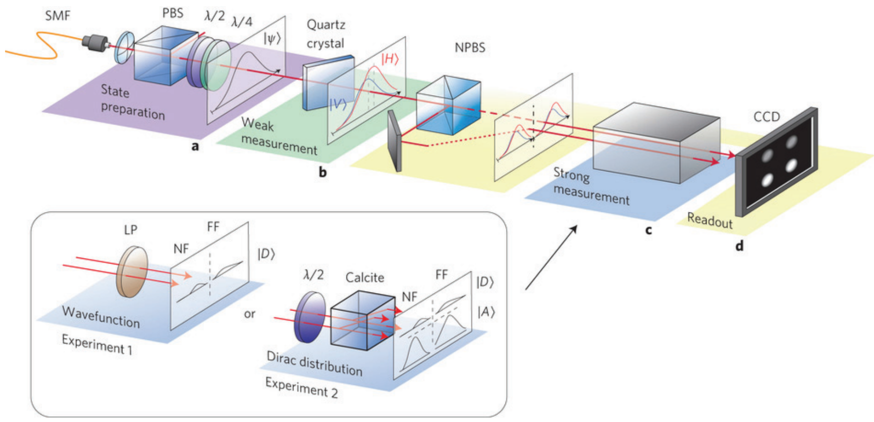

Fig. 12. – Experimental setup utilized for the characterization of polarization states of light via direct measurement. a) shows the state preparation that consists of a Gaussian transverse mode in a polarization state created by a PBS, a HWP and a QWP. b) The weak perturbation is performed by a quartz crystal at an oblique angle. c) The post-selection performed by a polarizer at a diagonal or anti-diagonal position. The authors also show the measurement required to reconstruct the Dirac distribution and the density matrix, which we do not discuss here. d) Shows how the shift in near and far-field of the pointer is imaged onto a CCD camera (figure adapted from ref. [24]).

As in the experiments discussed above, the definition of the weak value conveys an idea of the experimental implementation. Here, the probe is an unknown wave function $|\Psi\rangle$ that describes a polarization state of the form

$$|\Psi\rangle = \alpha\,|H\rangle + \beta\,|V\rangle\,, \tag{32}$$

where α and β are complex probability amplitudes and $|\alpha|^2 + |\beta|^2 = 1$. The pointer is the spatial profile of the beam which is a Gaussian mode. As in Ritchie's experiment [8], the weak perturbation is performed by introducing a small lateral displacement between the two polarization components of the beam; this is introduced by a quartz crystal at an oblique angle. The protocol is formalized with a post-selection in the polarization degree of freedom. A polarizer at either a diagonal or anti-diagonal position produces the following weak value

$$\langle \pi_H \rangle = \frac{\langle D|H\rangle\langle H|\Psi\rangle}{\langle D|\Psi\rangle} = \frac{\alpha}{\alpha - \beta}. \tag{33}$$

Equation (32) along with the relation between α and β, provide enough information to retrieve the complete wave function of the polarization qubit by performing a single post-selection. As shown in eqs. (8) and (9), the real part of the weak value can be determined by measuring the shift in the position of the pointer, whereas the imaginary component of the weak value is estimated through the shift in the momentum of the

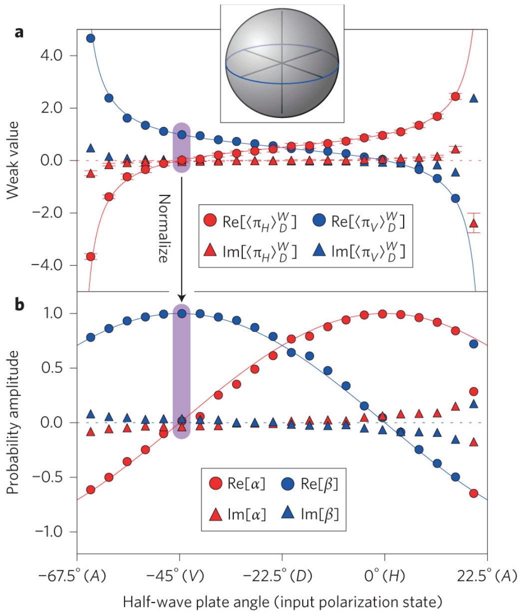

Fig. 13. – Experimental results for several input polarization states. a) Shows the real and imaginary part of the weak value. b) Shows the corresponding probability amplitudes given by the real and imaginary part of α and β (figure adapted from ref. [24]).

pointer. Therefore, the measurement of the centroid of the post-selected beam in the near and far-field allows the reconstruction of the initial polarization state.

The experimental setup is shown in fig. 12. A collimated Gaussian mode is prepared using a single mode fiber and a lens. A PBS, a HWP and a QWP allow the preparation of the polarization qubit. A quartz plate induces a net shift between the two polarization components of the beam. A non-polarizing beam splitter (NPBS) generates two copies of the perturbed state which are then post-selected by a polarizer at either diagonal or anti-diagonal position. The near-field and far-field of the post-selected beams are imaged onto a CCD camera. These measurements allow one to retrieve the polarization qubit. Figure 13 shows the real and imaginary components of the weak value and the corresponding probability amplitudes for different polarization qubits.

In addition, the authors have determined the density matrix of the system through the measurement of the elements of the Dirac distribution. However, this topic falls out of the scope of this paper and we will not discuss it here.

In this paper, we have discussed the distinction between strong and weak measurements. In addition, several applications of weak values were presented. We have also explained the physics behind the first realization of a weak value and its relation with some remarkable techniques for weak value amplification. In addition, the novel measurement procedure known as direct measurement was described. Finally, we presented some of the recent progress that our group has made on weak measurements, particularly we discussed weak value amplification in the azimuthal degree of freedom, compressive direct measurement, direct measurement in the OAM basis, and the full characterization of a polarization qubit.

* * *

The authors would like to thank Dr. Brandon Rodenburg, Dr. Seyed Mohammad Hashemi Rafsanjani, Dr. Mehul Malik, Dr. Martin Lavery, Jeff Salvail, Megan Agnew, Allan Johnson, Eliot Bolduc, Prof. Jonathan Leach, Prof. Miles Padgett for their contributions to many of the experiments that we have discussed in this article. This work was supported by the DARPA/DSO InPho program, the Canadian Excellence Research Chair (CERC) program, and CONACyT. OSML also acknowledges support from the Società Italiana di Fisica.

REFERENCES

[1] Jacobs K., *Quantum Measurement Theory and its Applications* (Cambridge University Press, Cambridge) 2014.

[2] Aharonov Y., Albert D. and Vaidman L., *Phys. Rev. Lett.*, **60** (1988) 1351.

[3] Sokolovski D., Msezane A. Z. and Shaginyan V. R., *Phys. Rev. A*, **71** (2005) 064103.

[4] Lundeen J. S., Sutherland B., Patel A., C. S. and Bamber C., *Nature*, **474** (2011) 188.

[5] Steinberg A. M., *Phys. Rev. Lett.*, **74** (1995) 2405.

[6] Aharonov Y., Botero A., Popescu S. and Reznik B., *Phys. Lett. A*, **301** (2002) 130.

[7] Kocsis S., Braverman B., Ravets S., Stevens M. J., Mirin R. P., Shalm L. K. and Steinberg A. M., *Science*, **332** (2011) 1170.

[8] Ritchie N., Story J. and Hulet R., *Phys. Rev. Lett.*, **66** (1991) 1107.

[9] Dressel J., Malik M., Miatto F. M., Jordan A. N. and Boyd R. W., *Rev. Mod. Phys.*, **86** (2014) 307.

[10] Botero A. and Reznik B., *Phys. Rev. A*, **61** (2000) 050301.

[11] Brunner N., Acin A., Collins D., Gisin N. and Scarani V., *Phys. Rev. Lett.*, **91** (2003) 180402.

[12] Feizpour A., Xing X. and Steinberg A. M., *Phys. Rev. Lett.*, **107** (2011) 133603.

[13] Viza G. I., Martínez-Rincón J., Howland G. A., Frostig H., Shomroni I., Dayan B. and Howell J. C., *Opt. Lett.*, **38** (2013) 2949.

[14] Hofmann H. F., *Phys. Rev. A*, **83** (2011) 022106.

[15] Brunner N. and Simon C., *Phys. Rev. Lett.*, **105** (2010) 010405.

[16] Hosten O. and Kwiat P., *Science*, **319** (2008) 787.

[17] Xu X.-Y., Kedem Y., Sun K., Vaidman L., Li C.-F. and Guo G.-C., *Phys. Rev. Lett.*, **111** (2013) 033604.

[18] Strübi G. and Bruder C., *Phys. Rev. Lett.*, **110** (2013) 083605.

[19] Salazar-Serrano L. J., Janner D., Brunner N. and Pruneri V., *Phys. Rev. A*, **89** (2014) 012126.

[20] Dixon P., Starling D. J., Jordan A. N. and Howell J. C., *Phys. Rev. Lett.*, **102** (2009) 173601.

[21] Magaña-Loaiza O. S., Mirhosseini M., Rodenburg B. and Boyd R. W., *Phys. Rev. Lett.*, **112** (2014) 200401.

[22] Malik M., Mirhosseini M., Lavery M. P. J., Leach J., Padgett M. J. and Boyd R. W., *Nat. Commun.*, **5** (2014) 3115.
[23] Hofmann H. F., *Phys. Rev. A*, **81** (2010) 012103.
[24] Salvail J. Z., Agnew M., Johnson A. S., Bolduc E., Leach J. and Boyd R. W., *Nat. Photon.*, **7** (2013) 316.
[25] Mirhosseini M., Magaña-Loaiza O. S., Hashemi Rafsanjani S. M. and Boyd R. W., *Phys. Rev. Lett.*, **113** (2014) 090402.
[26] Ferrie C. and Combes J., *Phys. Rev. Lett.*, **112** (2014) 040406.
[27] Knee G. C. and Gauger E. M., *Phys. Rev. X*, **4** (2014) 011031.
[28] Qian X. F. and Eberly J. H., *Opt. Lett.*, **36** (2011) 4110.
[29] Kagalwala K. H., Di Giuseppe G., Abouraddy A. F. and Saleh B. E. A., *Nat. Photon.*, **7** (2012) 72.
[30] Johansen L. M., *Phys. Rev. Lett.*, **93** (2004) 120402.
[31] Puentes G., Hermosa N. and Torres J. P., *Phys. Rev. Lett.*, **109** (2012) 040401.
[32] Lundeen J. S. and Resch K. J., *Phys. Lett. A*, **334** (2005) 337.
[33] Jozsa R., *Phys. Rev. A*, **76** (2007) 044103.
[34] Mirhosseini M., Viza G., Magaña Loaiza O. S., Malik M., Howell J. C. and Boyd R. W., arXiv, quant-ph (2014).
[35] Jordan A. N., Martínez-Rincón J. and Howell J. C., *Phys. Rev. X*, **4** (2014) 011031.
[36] Giovannetti V., Lloyd S. and Maccone L., *Nat. Photon.*, **5** (2011) 222.
[37] Thomas-Peter N., Smith B. J., Datta A., Zhang L., Dorner U. and Walmsley I. A., *Phys. Rev. Lett.*, **107** (2011) 113603.
[38] Shin H., Magaña-Loaiza O. S. and Malik M., *Opt. Express*, **21** (2013) 2816.
[39] Allen L., Beijersbergen M. W., Spreeuw R. J. C. and Woerdman J. P., *Phys. Rev. A*, **45** (1992) 8185.
[40] Courtial J., Robertson D. A., Dholakia K. and Allen L., *Phys. Rev. Lett.*, **81** (1998) 4828.
[41] Lavery M. P. J., Speirits F. C., Barnett S. M. and Padgett M. J., *Science*, **341** (2013) 537.
[42] D'Ambrosio V., Spagnolo N., Del Re L., Slussarenko S., Li Y., Kwek L. C., Marrucci L., Walborn S. P., Aolita L. and Sciarrino F., *Nat. Commun.*, **4** (2013) 2432.
[43] Fickler R., Lapkiewicz R., Plick W. N., Krenn M., Schaeff C., Ramelow S. and Zeilinger A., *Science*, **338** (2012) 640.
[44] Jha A. K., Agarwal G. S. and Boyd R. W., *Phys. Rev. A*, **83** (2011) 053829.
[45] Davis J. A., Cottrell D. M., Campos J., Yzuel M. J. and Moreno I., *Appl. Opt.*, **38** (1999) 5004.
[46] Nagali E., Sciarrino F., Francesco De M., Lorenzo M., Piccirillo B., Karimi E. and Santamato E., *Phys. Rev. Lett.*, **103** (2009) 013601.
[47] Romberg J., *IEEE Signal Process. Mag.*, **25** (2008) 14.
[48] Candes E. and Romberg J., *Inverse Probl.*, **23** (2007) 969.
[49] Malik M., Magaña-Loaiza O. S. and Boyd R. W., *Appl. Phys. Lett.*, **101** (2012) 241103.
[50] Aspden R. S., Tasca D. S., Boyd R. W. and Padgett M.,. *New J. Phys.*, **15** (2013) 073032.
[51] Katz O., Bromberg Y. and Silberberg Y., *Appl. Phys. Lett.*, **95** (2009) 131110.
[52] Zerom P., Clifford Chan K.-W., Howell J. C. and Boyd R. W., *Phys. Rev. A*, **84** (2011) 061804.
[53] Magaña-Loaiza O. S., Howland G. A., Malik M., Howell J. C. and Boyd R. W., *Appl. Phys. Lett.*, **102** (2013) 231104.

[54] LIU W.-T., ZANG T., LIU J.-Y., CHEN P.-X. and YUAN J.-M., *Phys. Rev. Lett.*, **108** (2012) 170403.
[55] HOWLAND G. A. and HOWELL J. C., *Phys. Rev. X*, **3** (2013) 011013.
[56] LI C., YIN W. and ZHANG Y., *User's guide for TVAL3:TV minimization by augmented Lagrangian and alternating direction algorithms* (Rice University) 2010.
[57] RAYMER M. G., BECK M. and MCALISTER D., *Phys. Rev. Lett.*, **72** (1994) 1137.
[58] JAMES D. F. V., KWIAT P. G., MUNRO W. J. and WHITE A. G., *Phys. Rev. A*, **64** (2001) 052312.
[59] MAIR A., VAZIRI A., WEIHS G. and ZEILINGER A., *Nature*, **412** (2001) 313.
[60] LEACH J., PADGETT M. J., BARNETT S. M., FRANKE-ARNOLD S. and COURTIAL J., *Phys. Rev. Lett.*, **88** (2002) 257901.
[61] BERKHOUT G. C. G., LAVERY M. P. J., COURTIAL J., BEIJERSBERGEN M. W. and PADGETT M. J., *Phys. Rev. Lett.*, **105** (2010) 153601.
[62] MIRHOSSEINI M., MALIK M., SHI Z. and BOYD R. W., *Nat. Commun.*, **4** (2013) 2781.
[63] FRANKE-ARNOLD S., ALLEN L. and P. M., *Laser Photon. Rev.*, **2** (2008) 299.
[64] PADGETT M. and BOWMAN R., *Nat. Photon.*, **5** (2011) 343.
[65] MIRHOSSEINI M., MAGAÑA-LOAIZA O. S., O'SULLIVAN M. N., RODENBURG B., MALIK M., LAVERY M. P. J., PADGETT M. J., GAUTHIER D. J. and BOYD R. W., *New J. Phys.*, **17** (2015) 033033.
[66] RODENBURG B., MIRHOSSEINI M., MALIK M., MAGAÑA-LOAIZA O. S., YANAKAS M., MAHER L., STEINHOFF N. K., TYLER G. A. and BOYD R. W., *New J. Phys.*, **16** (2014) 033020.
[67] BARNETT S. M., *Phys. Rev. A*, **41** (1990) 3427.